Journal of Electromagnetic Waves and Applications

ISSN: 0920-5071 (Print) 1569-3937 (Online) Journal homepage: https://www.tandfonline.com/loi/tewa20

Dual-band multiple-input multiple-output antenna based on half split cylindrical dielectric resonator

Abhishek Sharma, Anirban Sarkar, Animesh Biswas & M. Jaleel Akhtar

To cite this article: Abhishek Sharma, Anirban Sarkar, Animesh Biswas & M. Jaleel Akhtar (2018) Dual-band multiple-input multiple-output antenna based on half split cylindrical dielectric resonator, Journal of Electromagnetic Waves and Applications, 32:9, 1152-1163, DOI: 10.1080/09205071.2018.1425159

To link to this article: https://doi.org/10.1080/09205071.2018.1425159

Published online: 12 Feb 2018.

JOURNAL OF ELECTROMAGNETIC WAVES AND APPLICATIONS, 2018
VOL. 32, NO. 9, 1152–1163
https://doi.org/10.1080/09205071.2018.1425159

Taylor & Francis
Taylor & Francis Group

Dual-band multiple-input multiple-output antenna based on half split cylindrical dielectric resonator

Abhishek Sharma, Anirban Sarkar, Animesh Biswas and M. Jaleel Akhtar

Department of Electrical Engineering, Indian Institute of Technology Kanpur, Kanpur, India

ABSTRACT

In this article, a dual-band half split cylindrical dielectric resonator antenna is proposed for multiple-input multiple-output (MIMO) applications. The dual-band operation is achieved by simultaneously exciting $TE_{01\delta}$ and $TE_{02\delta}$ modes in an aperture coupled fed half split cylindrical dielectric resonator. The topology of four element MIMO antenna is such that it provides both spatial and polarization diversities. Over both the operating bands, the measured port-to-port isolation is better than 20 dB. The proposed antenna exhibits broadside radiation with cross polarization level below −15 dB in both *xz*- and *yz*-plane. The peak gain of antenna is 4.88 and 5.32 dBi at lower and upper operating frequency, respectively. The MIMO performance of the proposed antenna is found to be good with ECC<0.06. Moreover, the channel capacity of the proposed MIMO is near to uncorrelated case for uniform propagation scenario. The proposed antenna could be suitable for LTE 22/LTE 42 and WLAN applications.

ARTICLE HISTORY
Received 25 August 2017
Accepted 28 December 2017

KEYWORDS
Dielectric resonator antenna; LTE; polarization diversity; multiple-input multiple-output; spatial diversity; WLAN

1. Introduction

With the rapid advancement in wireless communication systems, there is an overwhelming demand for high bit rate and high-quality data transmission. In order to cater to these demands, the requirement of multi antenna systems or multiple-input multiple-output (MIMO) systems is indispensable. The MIMO technology utilizes multiple radiators at transmitting and receiving ends that greatly enhance the channel capacity without additional power requirement with improved link reliability [1]. In present scenario, the MIMO has become incredibly popular and finds application in wireless communications, such as Long-Term Evolution (LTE), Worldwide Interoperability for Microwave Access (WiMAX) systems or Wireless Local Area Networks (WLANs). Additionally, the multi-band MIMO antennas are needed in order to meet the emerging requirements of multi-standard modern wireless communication systems. Over the past few years, a considerable amount of research has been dedicated to design printed multi-band diversity and MIMO antennas for numerous wireless communication systems [2–5].

On the other hand, dielectric resonator antennas (DRAs) have received widespread attention due to their potential advantages such as high radiation efficiency (due to lack of surface wave and conductor losses), low dissipation loss, ease of excitation, high degree

CONTACT Abhishek Sharma abhisheksharma.rf@gmail.com, sharma@iitk.ac.in

of design flexibility etc [6]. Moreover, different modes with distinct radiation characteristics can be excited within a single dielectric resonator (DR) which makes it a potential candidate for diversity applications. Therefore, DRAs are now being introduced as a viable alternative of conventional printed/metallic antennas for implementing diversity and MIMO systems. In the past, several DR-based MIMO antennas have been investigated for single band and wideband operation covering both microwave and millimeter-wave frequency band [7–11]. Some investigations have also been carried out for DR-based multi-band MIMO antenna system. For instance, in [12], a multi-band dielectric resonator antenna with pattern diversity has been proposed for different wireless applications (DVB-H-800MHz/Wi-Fi-2.4 GHz/WiMAX−3.5 GHz). However, the isolation achieved between the ports is poor as well as the ECC≈0.3 at the lower band. In [13], the dual-band and wideband dual polarized DRAs have been designed by utilizing HEM_{111} and HEM_{113} mode of cylindrical DR for DCS and WLAN applications and in the proposed design the matching at one of the port is done using parasitic. A low profile, eight-element (four elements for each band) dual-band MIMO DRA for wireless access points has been presented in [14]. However, this technique results in larger antenna footprint and in order to reduce correlation an extra metallic reflector has been used. In [15], L-shaped dual-band MIMO DRA has been investigated for WiMAX and WLAN applications. The isolation achieved was about 10 dB which was somewhat improved using a defected ground structure. Moreover, a metallic strip has been used to improve matching and the antenna also suffers from high level of cross polarization at higher frequency band. In another work [16], authors have designed a dual-band MIMO rectangular DRA for LTE band applications. Though, the high isolation has been achieved by using hybrid feeding mechanism and separate ground planes, however, the separate ground planes cannot be used practically in the real system as addressed in [17]. A quad-element multi-band antenna using dielectric resonator and a radiating patch with meander line has been proposed for LTE MIMO operations in [18], howbeit, the isolation achieved was poor with the worst isolation equal to 6 dB.

From above discussion, it can be inferred that most of the dual-band MIMO DRA design utilized either two-element or two-port antenna configuration. However, a MIMO system with more than two antenna elements can provides larger channel capacity and better link reliability, which is very much needed in the present scenario of wireless communication technology. It is mainly due to this reason that in this paper, a four element dual-band MIMO antenna based on dielectric resonator is proposed. In the proposed design, the higher order mode design approach [19,20] is used to design dual-band DRA which does not require any additional DR element and also facilitates the matching of dual-band antenna. Additionally, this approach makes the design simpler. The antenna element used in the proposed design is similar to the element used in [7]. However, in [7] two different modes *viz.* $TE_{011+\delta}$ and $HE_{11\delta}$ were excited simultaneously using dual ports and the resonant frequency of both the modes were different. But in order to work in a MIMO system, both the modes should have same resonant frequency and therefore, for mode degeneracy the authors have applied boundary perturbation. The design presented in [7] is a single-band dual port MIMO system. Howbeit, in the proposed work, two modes viz. $TE_{01\delta}$ and $TE_{02\delta}$ are simultaneously excited in half split cylindrical DR using aperture coupled feeding mechanism to achieve the dual-band response. Furthermore, a quad element MIMO system is implemented using the proposed dual-band DRA which offer both spatial and polarization diversities with good

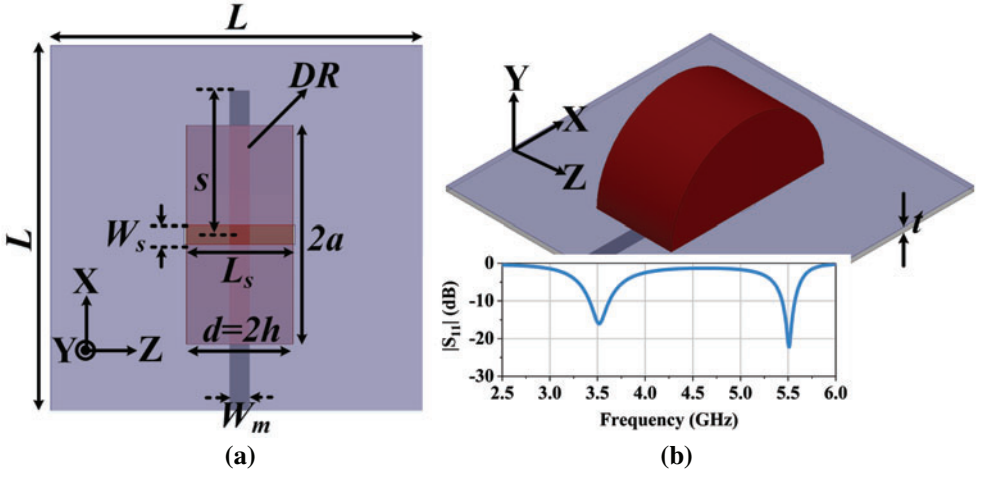

Figure 1. Geometry of the proposed antenna (a) top view (b) isometric view ($L = 45, a = 13, d = 12.7, L_s = 13.2, W_m = 2.36, W_s = 2.3, s = 17.1, t = 0.787$, all dimensions are in mm).

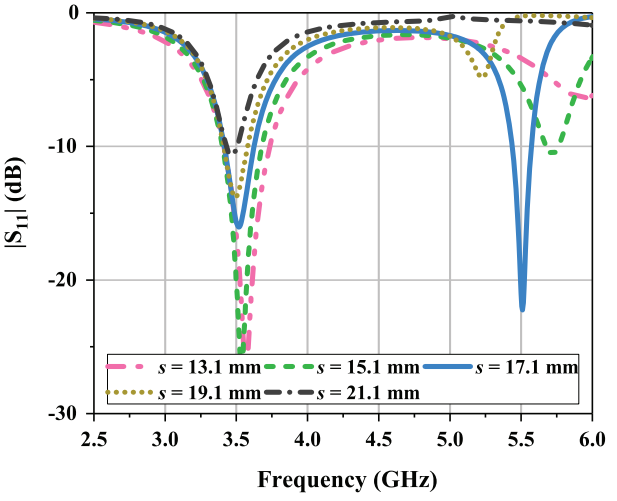

Figure 2. Effect of stub length on reflection coefficient of the dual-band DRA.

isolation and diversity performance. All simulations are done in HFSS and a prototype of same is built and experimentally verified.

2. Dual-band half split cylindrical DRA

Figure 1 shows the top and isometric view of half split cylindrical DRA. A 50Ω microstrip line of width W_m printed on a low permittivity substrate (dielectric constant 2.2 and thickness 0.787 mm) couples the energy to the half split cylindrical DR via an aperture of dimension $L_s \times W_s$. The DR under investigation is made from Rogers RT/Duroid 6010 of relative permittivity 10.2.

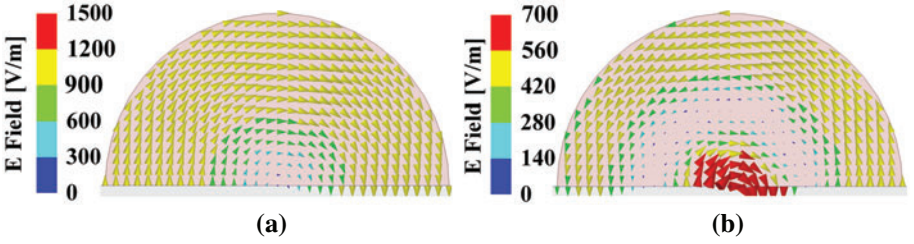

Figure 3. Electric field distributions in *xy*-plane at (a) 3.5 GHz (b) 5.5 GHz.

2.1. Design equations

The aperture feeding mechanism results in $TE_{01\delta}$ mode excitation which radiates like a short horizontal magnetic dipole. The resonant frequency of the $TE_{01\delta}$ mode of the cylindrical DRA can be calculated as [6]

$$k_0 a = \frac{2.327}{\sqrt{\epsilon_r + 1}} \left(1 + 0.2123\frac{a}{h} - 0.00898\left(\frac{a}{h}\right)^2\right) \tag{1}$$

The same equation can be used to calculate the resonant frequency of the half split cylindrical DRA with $d = 2h$. The initial value of the slot length L_s, slot width W_s and stub length s are chosen as [6]

$$L_s = \frac{0.4\lambda_0}{\sqrt{\epsilon_e}} \quad \epsilon_e = \frac{\epsilon_r + \epsilon_s}{2} \tag{2}$$

$$W_s = 0.2L_s \tag{3}$$

$$s = \frac{\lambda_g}{4} \tag{4}$$

where, ϵ_r and ϵ_s are the dielectric constants of the DRA and substrate, λ_g is the guided wavelength. These feed parameters are then optimized further through simulations such that good matching can be achieved to obtain dual-band operation. Figure 2 shows the reflection coefficient for the different values of stub length *s*. From the figure, it is observed that the better matching is achieved for the stub length of 17.1 mm.

The theoretical resonant frequency for $TE_{01\delta}$ mode calculated using the Equation (5) is 3.6 GHz, which agrees with the simulated value of 3.5 GHz. The dual-band antenna is operating at 3.5 GHz with impedance bandwidth (IBW, for $S_{11} < -10$ dB) of 6.3% (3.4–3.62 GHz) and 5.5 GHz with impedance bandwidth of 2.4% (5.44–5.57 GHz).

2.2. Electric field distribution

In order to verify the excitation of above modes, modal electric field distribution is portrayed in Figure 3 at 3.5 and 5.5 GHz. It is clear from the field distribution that the $TE_{01\delta}$ mode is excited at 3.5 GHz while the $TE_{02\delta}$ is excited at 5.5 GHz. Both the modes show similar radiation pattern along the broadside direction.

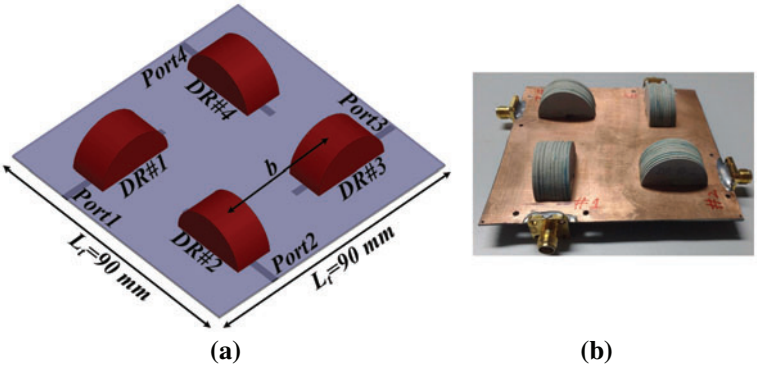

Figure 4. (a) Proposed four element dual-band MIMO dielectric resonator antenna (b) Fabricated prototype.

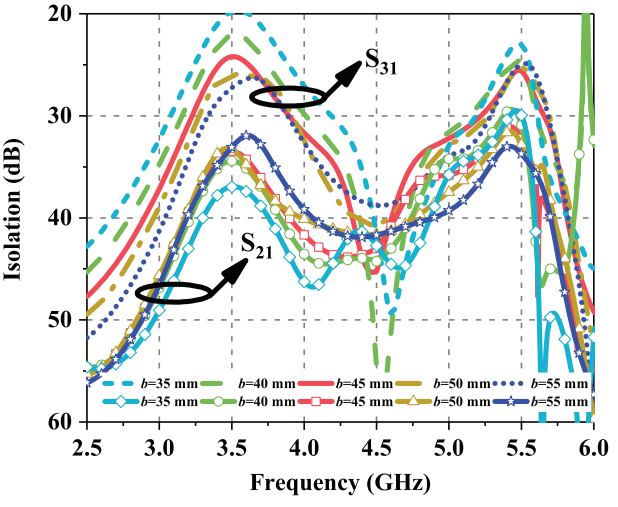

Figure 5. Simulated isolation for different values of inter element spacing *b*.

3. Four-element dual-band MIMO system

3.1. Impedance performance

The proposed four-element dual-band MIMO DRA is depicted in Figure 4. The antenna element pairs (1, 3) and (2, 4) provides spatial diversity whereas the orthogonal placement of the pairs (1, 2) and (1, 4) result into polarization diversity. Figure 5 shows the isolation curves for different values of the inter element spacing *b*. For the present design, the inter element spacing *b* is chosen as 45 mm in order to ensure the minimum isolation of 25 dB.

The simulated and measured reflection coefficient and isolation of the proposed MIMO DRA are shown in Figure 6. From the simulation, it is evident that the proposed antenna operates at 3.5 GHz (IBW 6.6%) and 5.5 GHz (IBW 2.56%) for all the four ports. The measured results show that the antenna operates at 3.27 GHz (IBW 5.52%) and 5.40 GHz (IBW 2.97%)

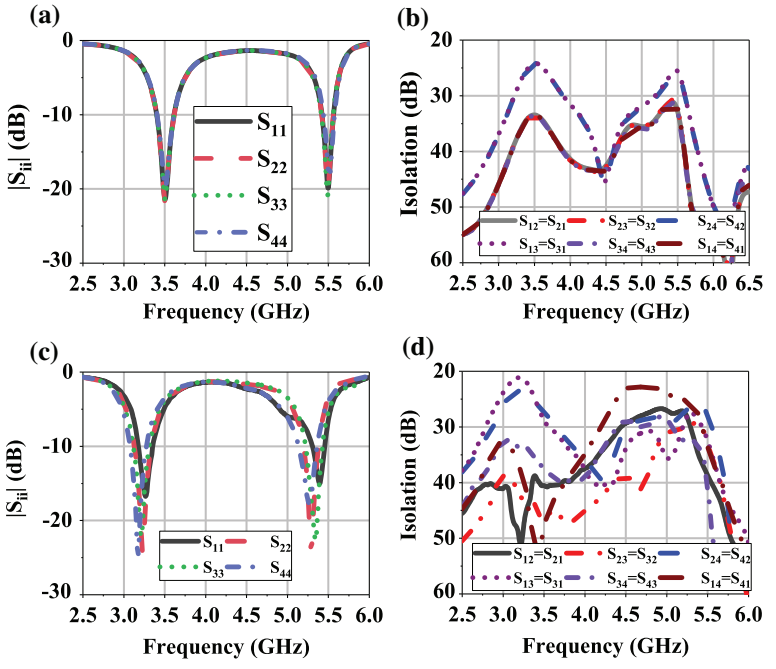

Figure 6. Response of the proposed dual-band MIMO DRA (a) Simulated reflection coefficient (b) Simulated isolation (c) Measured reflection coefficient (d) Measured isolation.

for Port1; at 3.22 GHz (IBW 6.51%) and 5.30 GHz (IBW 3.6%) for Port2; at 3.21 GHz (IBW 6.23%) and 5.34 GHz (IBW 3.94%) for Port3; at 3.17 GHz (IBW 6.61%) and 5.26 GHz (IBW 4.38%) for Port4. Over the two operating bands, both the simulated and measured isolation between the input ports is better than 20 dB. The disagreement between the simulated and measured results can be attributed to fabrication tolerances, alignment of DR and inevitable air gap between the DR and the ground plane. Though, a very thin layer of adhesive is used to bond the DR on ground plane but it might affect the measurement as well.

3.2. Radiation performance

The simulated and measured normalized radiation pattern of the antenna element *DR#1* (Port 1) in *xz*- and *yz*-plane with Port 2 to Port 4 terminated with matched load are depicted in Figure 7. As expected, the antenna radiates along the broadside direction and the cross polarization level is better than −15 dB in both simulation and measurement. The simulated and measured peak gain of the proposed MIMO antenna is 5.20 and 4.88 dBi, respectively, at lower operating frequency and 5.85 and 5.32 dBi, respectively, at upper operating frequency. The remaining three antenna elements i.e. *DR#2*, *DR#3* and *DR#4* behave in similar manner and therefore, their radiation pattern plots are not shown for brevity.

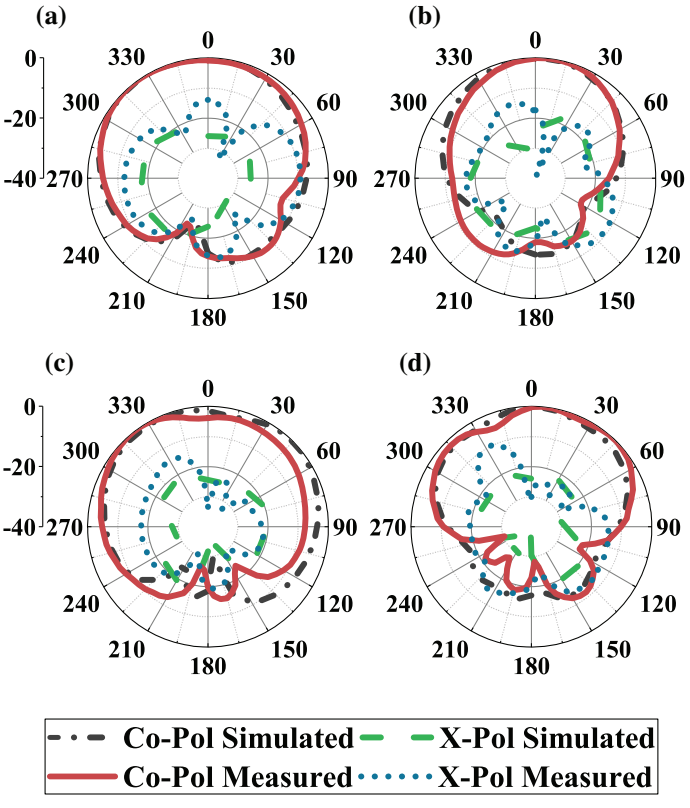

Figure 7. Normalized radiation pattern of element *DR#1* with Port2 to Port4 terminated with matched loads (a) *yz*-plane at f_L (b) *xz*-Plane at f_L (c) *yz*-Plane at f_U (d) *xz*-Plane at f_U (f_L: Lower operating frequency and f_U: Upper operating frequency).

3.3. MIMO performance

The proposed MIMO antenna is intended to be use in rich scattering environment. Thus, to evaluate its performance, the envelope correlation coefficient (ECC), total active reflection coefficient, and channel capacity are studied.

3.3.1. Envelope correlation coefficient

ECC describes how the communication channels are isolated or correlated with each other. This takes into account the radiation pattern of the antenna and delineate how much the radiation pattern in multi antenna systems affect each other. Assuming uniform propagation scenario, ECC between the i^{th} and j^{th} antenna elements can be computed as [2]

$$\rho_{e,ij} = \frac{|\int\int_{4\pi}(\vec{F}_i(\theta,\phi) * \vec{F}_j(\theta,\phi))\mathrm{d}\Omega|^2}{\int\int_{4\pi}|\vec{F}_i(\theta,\phi)|^2\mathrm{d}\Omega\int\int_{4\pi}|\vec{F}_j(\theta,\phi)|^2\mathrm{d}\Omega} \tag{5}$$

where $\vec{F}_i(\theta,\phi)$ denotes the three-dimensional radiation pattern function when port *i* of the MIMO antenna system is excited, Ω denotes the solid angle and represents the Hermitian product operator. The values of ECC computed using (5) for two operating frequencies are given in Table 1. ECC can also be determined through post-processing of scattering parameters of MIMO antenna system. For highly efficient antennas, port and field-based ECC

Table 1. ECC values calculated using (5).

Frequency (GHz)	ρ_{e12}	ρ_{e13}	ρ_{e14}	ρ_{e23}	ρ_{e24}	ρ_{e34}
3.5	0.0009	0.0511	0.0008	0.0009	0.0534	0.0008
5.5	0.0008	0.0096	0.0011	0.0012	0.0108	0.0007

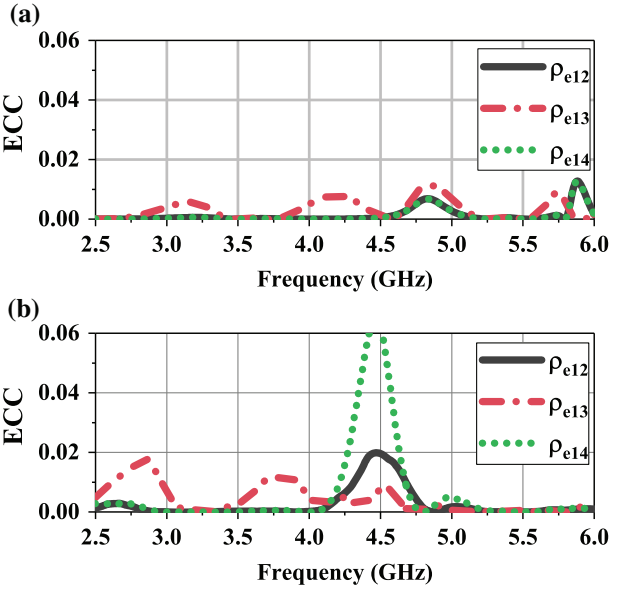

Figure 8. Variation of ECC with frequency (a) Simulated (b) Measured.

calculations shows a reasonable agreement between two sets of values [10]. Under certain assumptions, ECC between *i*th and *j*th elements can be calculated for N-port antennas system as [8]

$$\rho_{eij} = \frac{\left|\sum_{n=1}^{N} S_{in}^{*} S_{nj}\right|^{2}}{\prod_{k=i,j}\left[1 - \sum_{n=1}^{N} S_{kn}^{*} S_{nk}\right]} \tag{6}$$

where, S_{ij} is the S-parameters of MIMO system and $\{\cdot\}^{*}$ denotes the complex conjugate. Figure 8 shows the simulated and measured variation in ECC. From Table 1, it is observed that ECC values are below 0.06 at both the operating frequencies, which lies within the acceptable limit (ECC<0.3 [2]), indicating effective diversity performance.

3.3.2. Total active reflection coefficient

Total active reflection coefficient (TARC) is used to characterize the bandwidth and radiation performance of the multiport antenna. It accounts the mutual coupling between the elements and random-signal combinations between the ports. TARC is defined as the ratio of square root of total reflected power to the square root of total incident power [2]

$$\Gamma_{a}^{t} = \frac{\sqrt{\sum_{i=1}^{N} |b_i|^2}}{\sqrt{\sum_{i=1}^{N} |a_i|^2}} \tag{7}$$

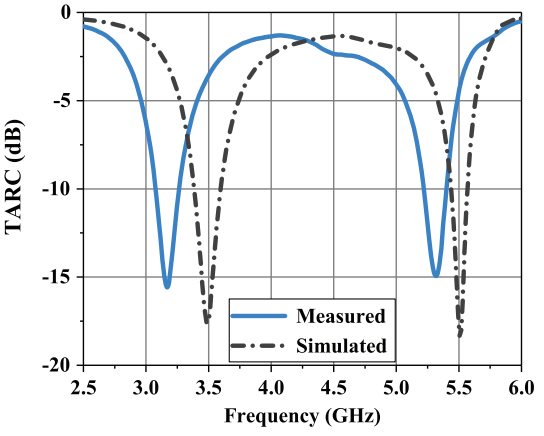

Figure 9. Simulated and measured average TARC for the proposed antenna.

Here, N is total number of antenna elements, a_i is the incident signal, b_i is the reflected signal and both are related with S-parameters as $\mathbf{b} = [S]\mathbf{a}$. Figure 9 shows the simulated and measured variation of average TARC of the proposed antenna. The TARC curve retains the original characteristics of reflection coefficient of single antenna with a slight change in the bandwidth. It is evident that TARC<-10 dB in both the working bands, showing good radiation performance and low mutual coupling.

3.3.3. Channel capacity

The highest rate of information that can be transmitted through the channel is known as capacity. Mathematically, the channel capacity for a given SNR is expressed as [21]

$$C = \log_2\left[\det\left(\mathbf{I}_{N_r} + \frac{\gamma}{N_t}\mathbf{H}\mathbf{H}^{\dagger}\right)\right] \tag{8}$$

where N_r is the number of receiving antennas, N_t is the number of transmitting antennas, $\mathbf{I}_{N_r}$ is the $N_r \times N_r$ identity matrix, γ is the averaged received signal to noise ratio (SNR), $\mathbf{H}$ is the normalized channel matrix and $\{\cdot\}^{\dagger}$ denotes Hermitian transpose. Generally speaking, in the multi antenna system, the entries of $\mathbf{H}$ are correlated. Considering the simple Kronecker model, channel matrix can be defined as [21]

$$\mathbf{H} = \boldsymbol{\Psi}_r^{1/2}\boldsymbol{\Lambda}\boldsymbol{\Psi}_t^{1/2} \tag{9}$$

where $\boldsymbol{\Psi}_r$ and $\boldsymbol{\Psi}_t$ are the receive and transmit correlation matrix, respectively, and $\boldsymbol{\Lambda}$ is a random matrix with independently identical distributed (i.i.d) complex Gaussian entries and $\{\cdot\}^{1/2}$ denotes the square root of the matrix. Considering a 4×4 (four transmitter and four receiver) MIMO system, the channel capacity at both the operating frequency is computed using (8)–(9) and results are depicted in Figure 10. It is observed that the proposed MIMO antenna offers the capacity close to ideal (i.e. uncorrelated) case for uniform propagation scenario.

Table 2 shows a comparative study of the proposed MIMO antenna with the earlier reported dual-band MIMO DRAs. The proposed antenna has four elements that will provide

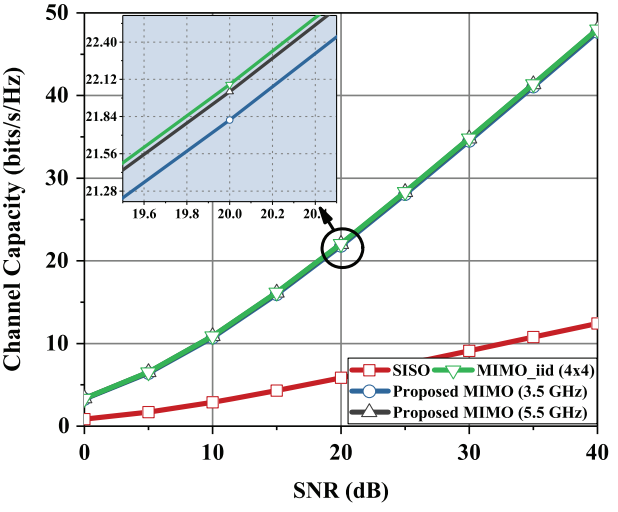

Figure 10. Channel capacity of proposed MIMO antenna as a function of SNR.

Table 2. Comparison of proposed antenna with other dual-band DRAs.

Ant.	No. of elements/ports	Operating frequency (GHz)	Minimum isolation (dB)	Design	Separate ground plane
		0.8	5		
[12]	2	2.4	14	Complex	No
		3.5	10		
		1.8			
[13]	2	2.4	40	Easy	No
		2.45			
[14]	4†	5.8	15	Complex	No
		3.6	12		
[15]	2	5.2	15	Complex	No
		1.5	23		
[16]	2	2.8	32	Easy	Yes‡
		0.75–0.96	6		
[18]	4	1.7–3.6	12	Easy	No
	4	**3.5**			
This work	**4**	**5.5**	**22**	**Easy**	**No**

†4 elements for each band, ‡Not desirable. Bold values signifies the design parameters of the proposed antenna.

higher capacity than the dual-element MIMO system. Moreover, as compared to [12,14,15, 18], the proposed antenna has higher isolation. It can be easily observed from the table that the proposed antenna has better isolation, more number of elements and less design complexity as compared to the earlier reported dual-band MIMO structures.

4. Simulation study of dual-band DRA having different aspect ratio (a/d)

In the present work, the dual-band is achieved by exciting higher order $TE_{02\delta}$ mode along with the fundamental $TE_{01\delta}$ mode by adjusting the stub length s of the microstrip feed line. This method can indeed be used to design dual-band half split cylindrical DRA having different aspect ratio (a/d). In order to validate this, two examples with $a/d = 0.86$ and

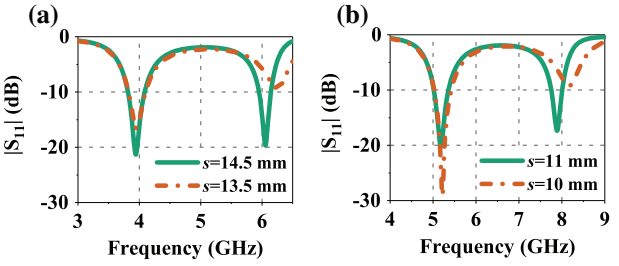

Figure 11. Simulated response for different aspect ratio of DR (a) $a = 11$ mm, $d = 12.7$ mm, $a/d = 0.86$, $W_s = 2$ mm, $L_s = 13.2$ mm (b) $a = 10$ mm, $d = 6$ mm, $a/d = 1.66$, $W_s = 1.6$ mm, $L_s = 10$ mm.

Table 3. Resonant frequencies of first and second mode.

a (mm)	d (mm)	a/d	$f_{1,\text{theoretical}}$ (GHz)	$f_{1,\text{simulated}}$ (GHz)	$f_{2,\text{simulated}}$ (GHz)
11	12.7	0.86	4.05	3.94	6.06
10	6	1.66	5.33	5.22	7.9

$a/d = 1.66$ are simulated and the results are shown in Figure 11. From the figure, it can clearly be seen that the dual-band behavior in half split cylindrical DRA can be achieved by adjusting the stub length s of the microstrip feed line irrespective of the aspect ratio. Table 3 summarizes the resonant frequencies of both the modes.

5. Conclusion

A four element dual-band dielectric resonator based MIMO antenna has been proposed which offers polarization as well as spatial diversities. The dual band behavior has been achieved by simultaneously exciting $TE_{01\delta}$ and $TE_{02\delta}$ mode in an aperture coupled fed half split cylindrical DR. Across both the operating bands, the isolation better than 20 dB has been achieved. The antenna exhibits broadside radiation having cross polarization level less than -15 dB in both xz-and yz-planes. The peak gain of 4.88 and 5.32 dBi has been obtained at lower and upper operating frequency, respectively. Results shows that the proposed antenna offers satisfactory diversity performance with ECC<0.06, which conforms to specified standard ($\rho_{eij} < 0.3$) for wireless communication system and the channel capacity of the proposed MIMO antenna is close to uncorrelated case under uniform propagation scenario. The antenna could be suitable for MIMO communication applications such as LTE and WLAN.

Disclosure statement

No potential conflict of interest was reported by the authors.

ORCID

Abhishek Sharma http://orcid.org/0000-0001-8026-9752

References

[1] Jensen MA, Wallace JW. A review of antennas and propoagation for MIMO wireless communications. IEEE Trans Antennas Propag. 2004;52:2810–2824.
[2] Sharawi MS. Printed MIMO antenna engineering. Artech House: Boston (MA); 2014.
[3] Wu YT, Chu QX. Dual-band multiple input multiple output antenna with slitted ground. IET Mirow Antennas Propag. 2014;8:1007–1013.
[4] Liao WJ, Hsieh CY, Dai BY, et al. Inverted-F/slot integrated dual-band four-antenna system for WLAN access points. IEEE Antennas Wireless Propag Lett. 2015;14:847–850.
[5] Sarkar D, Saurav K, Srivastava KV. A compact four element CSRR-loaded antenna for dual band pattern diversity MIMO applications. 46th European Microwave Conference (EuMC). London; 2016 Oct. p. 1315–1318.
[6] Petosa A. Dielectric resonator antenna handbook. Artech House: Boston (MA); 2007.
[7] Yan JB, Bernhard JT. Design of a MIMO dielectric resonator antenna for LTE femtocell base stations. IEEE Trans Antennas Propag. 2012;60:438–444.
[8] Fang X, Leung K, Luk K. Theory and experiment of three-port polarization-diversity cylindrical dielectric resonator antenna. IEEE Trans Antennas Propag. 2014;62:4945–4951.
[9] Roslan SF, Kamarudin MR, Khalily M, et al. An MIMO rectangular dielectric resonator antenna for 4G applications. IEEE Antennas Wireless Propag Lett. 2014;13:321–324.
[10] Sharawi MS, Podilchak SK, Hussain MT, et al. Dielectric resonator based MIMO antenna system enabling millimeter-wave mobile devices. IET Microw Antennas Propag. 2016;11:287–293.
[11] Sharma A, Biswas A. Wideband multiple-input-multiple-output dielectric resonator antenna. IET Microw Antennas Propag. 2017;11:496–502.
[12] Huitema L, Koubeissi M, Mouhamadou M, et al. Compact and multiband dielectric resonator antenna with pattern diversity for multistandard mobile handheld devices. IEEE Trans Antennas Propag. 2011;59:4201–4208.
[13] Sun YX, Leung KW. Dual-band and wideband dual-polarized cylindrical dielectric resonator antenas. IEEE Antennas Wireless Propag Lett. 2013;12:384–387.
[14] Sharawi MS, Podilchak SK, Khan MU, et al. Dual-frequency DRA-based MIMO antenna system for wireless access points. IET Microw Antennas Propag. 2017;11:1174–1182.
[15] Khan AA, Jamaluddin MH, Aqeel S, et al. Dual-band MIMO dielectric resonator antenna WiMAX/WLAN applications. IET Microw Antennas Propag. 2017;11:113–120.
[16] Khan AA, Khan R, Aqeel S, et al. Dual-band MIMO rectangular dielectric resonator antenna with high port isolation for LTE applications. Microw Optical Technol Lett. 2017;59:44–49.
[17] Sharawi MS. Current misuses and future prospects for printed multiple-input, multiple-output antenna systems. IEEE Antennas Propag Mag. 2017;59:162–170.
[18] Li K, Shi Y, Liang CH. Quad-element multiband antenna array in the smart mobile phone for LTE MIMO operations. Microw Opt Technol Lett. 2016;58:2619–2626.
[19] Sharma A, Biswas A. Dual-frequency half split cylindrical dielectric resonator antenna. 2015 IEEE Applied Electromagnetics Conference (AEMC), Guwahati, India. 2015 Dec, p. 1–2.
[20] Gupta P, Guha D, Kumar C. Dielectric resonator working as feed as well as antenna: new concept for dual-mode dual-band improved design. IEEE Trans Antennas Propag. 2016;64:1497–1502.
[21] Luo Y, Chu QX, Li JF, et al. A planar H-shaped directive antenna and its application in compact mimo antenna. IEEE Trans Antennas Propag. 2013;61:4810–4814.